Electronic Supplementary Material (ESI) for Energy & Environmental Science.

Supporting Information

Additive Engineering for High-Performance Room-Temperature-Processed Perovskite Absorbers with Micron-Size Grains and Microsecond-Range Carrier Lifetimes

Qiwei Han[ab], Yusong Bai[b], Jie Liu[acd], Ke-zhao Du[ab], Tianyang Li[ab], Dong Ji[b], Yihao Zhou[a], Changyong Cao[e], Donghyeop Shin[ab], Jie Ding[cd], Aaron D. Franklin[be], Jeffrey T. Glass[ae], Jinsong Hu[cd], Michael J. Therien[b], Jie Liu[*b], and David B. Mitzi[*ab]

[a]Department of Mechanical Engineering and Materials Science, Duke University, Durham, NC 27708, USA

[b]Department of Chemistry, Duke University, Durham, North Carolina 27708, USA

[c]Key Laboratory of Molecular Nanostructure and Nanotechnology, Institute of Chemistry, Chinese Academy of Science, 2 North 1st Street, Zhongguancun, Beijing, 100190, China.

[d]University of Chinese Academy of Science, Beijing 100049, China

[e]Department of Electrical and Computer Engineering, Duke University, Durham, North Carolina 27708, USA

Experimental

Film deposition methods

To prepare the pristine (no additives) precursor solution for $MAPbI_3$ films, 1.25 mmol methylammonium iodide (MAI) and 1.25 mmol lead iodide (PbI_2) were dissolved in 1 mL solvent containing N,N-dimethylformamide (DMF) and dimethyl sulfoxide (DMSO), with the volume ratio of DMF:DMSO = 9:1. To obtain the optimal $MAPbI_3$ films for high device performance at room temperature (i.e., RT-$MAPbI_3$), 40% MASCN and 5% extra PbI_2 (both are mol% relative to $MAPbI_3$) were added to the pristine precursor solution. The films were then deposited by spin-coating the precursor solution using a spin speed of 5000 r.m.p for 30 s, with a solvent dripping process (chlorobenzene used for the dripping step).[1, 2] The spin coating was performed in a nitrogen-filled glovebox with oxygen and water levels maintained below 0.1 ppm. The as-deposited $MAPbI_3$ films were dried in the glovebox anti-chamber at reduced pressure (Edwards RV12, maximum achievable vacuum is 2×10^{-3} mbar) for 20 min, to form the resultant films. For comparison, pristine $MAPbI_3$ (i.e., P-$MAPbI_3$) films were also prepared. The pristine $MAPbI_3$ precursor solution (no MASCN or extra PbI_2) was deposited with similar steps. After spin-coating, P-$MAPbI_3$ films were annealed on a hotplate at 100 ^{o}C for 10 min. To study the impact of MASCN level on room-temperature films, 0~50% MASCN together with 5% extra PbI_2 was added to the pristine $MAPbI_3$ precursor and the $MAPbI_3$ films were deposited with similar steps to those described above.

Device Fabrication

The FTO-coated glass substrates were cleaned in soapy water, deionized water, acetone and isopropanol with sonication and then all the substrates were baked at 500 ^{o}C in air for 1 hour before further use. To prepare the TiO_2 electron transport layers (ETLs), a precursor solution containing 2 ml ethanol and 4 ml titanium diisopropoxide bis(acetylacetonate) solution (75% wt. in isopropanol) was stirred at room temperature in air for 1 hour. The TiO_2 precursor solution was used to deposit the ~50 nm TiO_2 ETL by the hot spray pyrolysis method at 450 ^{o}C. The TiO_2 compact films were annealed in air at 500 ^{o}C for 1 hour. Then, the substrates were immersed in 0.02 M $TiCl_4$ water solution at 70 ^{o}C for 10 min. After the $TiCl_4$ treatment, substrates were dried by house compressed air and finally annealed at 500 ^{o}C in air for 1 hour. The $MAPbI_3$ films were deposited on the glass/FTO/TiO_2 substrates by following the procedure mentioned above. To complete the devices, Li-doped Spiro-OMeTAD was spin-coated on the $MAPbI_3$ films as the hole transport layer (HTL). A solution consisting of 75 mg Spiro-OMeTAD, 28.8 µL 4-tert-butylpyridine, 17.6 µL Li-bis(trifluoromethanesulfonyl)imide (Li-TFSI) solution (520mg Li-TFSI in 1mL acetonitrile) and 1 mL chlorobenzene was employed with a spin speed of 3000 r.m.p for 30s. Finally, Au was thermally evaporated on the HTL, with thickness of ~80 nm, to serve as the electrode.

Characterizations

Morphologies of the $MAPbI_3$ films were imaged with a scanning electron microscope (SEM, FEI XL30 SEM-FEG). Atomic force microscopy (AFM) images were characterized using a scanning probe microscope (Digital Instruments Dimension 3100). X-ray diffraction (XRD) measurements were carried out on a PANalytical Empyrean Powder X-ray diffractometer using CuKα radiation. The X-ray photoelectron spectroscopy (XPS) measurements were performed on an ESCALab220i-XL electron spectrometer (VG Scientific) using 300W Al K α radiation. Transmittance Infrared (IR) measurements were carried out employing a Fourier Transform Infrared (FTIR) spectrometer (Thermo Scientific Nicolet 380). The charge carrier lifetimes were characterized via time-resolved photoluminescence (TRPL) experiments using a Hamamatsu C4780 picosecond fluorescence lifetime measurement system (instrument response function ~150 ps). This system employs a Hamamatsu Streakscope C4334 as the photon-counting detector, and a Hamamatsu C4792-01 synchronous delay generator that electronically generates all time delays. A Hamamatsu 405 nm diode laser was utilized as the excitation source. Optical absorption measurements were performed on a Shimadzu UV-3600 spectrophotometer. The Tindall effect was tested with a commercial laser pen with red beam light (Beboncool RF 2.4 GHz). Dynamic light scattering (DLS) measurements were performed on a Zetasizer (Nano-ZS, Malvern Instruments). The external quantum efficiency (EQE) was taken using a QE-R instrument from Enlitech without bias voltage or illumination. The current density-voltage (*J*-*V*) characteristics and steady-state output were measured using a Keithley 2400 source meter. The illumination source was a Newport Oriel 92192 solar simulator with an AM1.5G filter, operating at 100 mW cm^{-2}. All devices were masked with area of 0.1 cm^{2} aperture to define the active areas. A standard silicon solar cell from Newport Corp. was used as reference for *J*-*V* and EQE measurements. All measurements were performed under ambient condition with relative humidity level of 35~55%.

Supplementary Figures

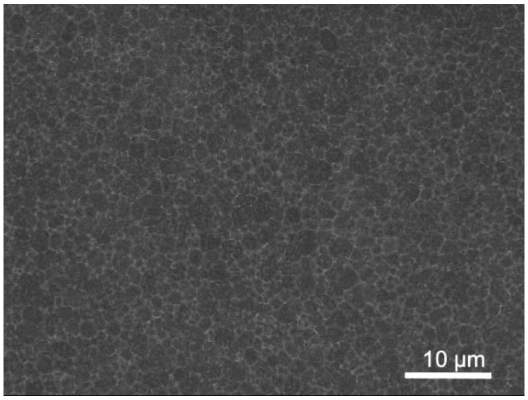

Fig. S1. Top-view SEM image (large scale) of the RT-$MAPbI_3$ film with 40% MASCN and 5% extra PbI_2 addition to the pristine $MAPbI_3$ precursor solution (mol% relative to stoichiometric $MAPbI_3$). The film was deposited on a glass/FTO/TiO_2 substrate. The films exhibit good uniformity with no evidence of pinholes.

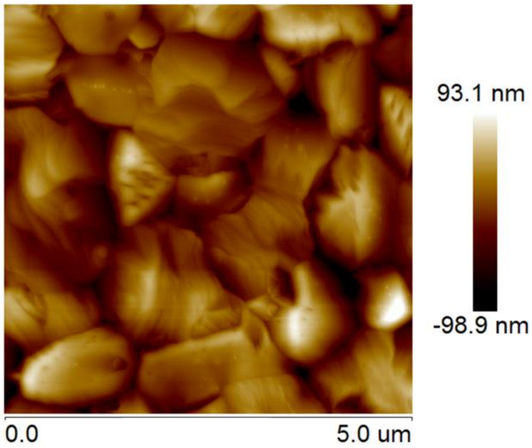

Fig. S2. Atomic force microscope (AFM) image of a RT-$MAPbI_3$ film. The extracted arithmetic average roughness is 21.80 nm. The film was deposited on a glass/FTO/TiO_2 substrate.

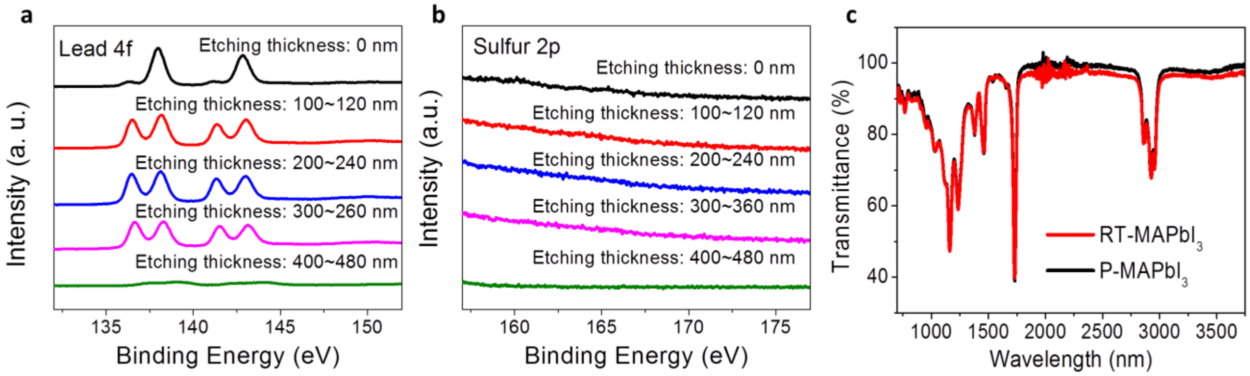

Fig. S3. a-b, XPS depth profiling results for the RT-$MAPbI_3$ film with 40% MASCN addition, in which the Pb 4f and S 2p peak are monitored at each etching thickness. The Pb 4f results are used to monitor when the back surface of the RT-$MAPbI_3$ has been reached. The S 2p results are used to indicate whether residual SCN^- and/or DMSO exist in the RT-$MAPbI_3$ film; **c,** Infrared (IR) spectra of RT- and A-$MAPbI_3$ films. The nearly overlapping spectra for the two films indicate identical chemical bonding in these two samples.

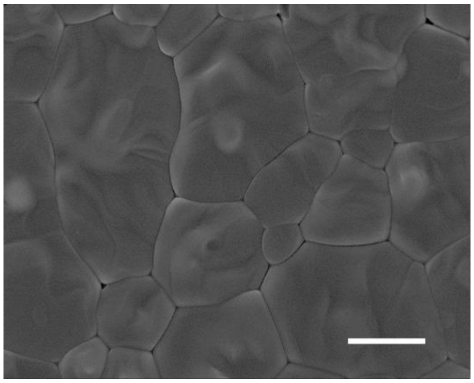

Fig. S4. Top-view SEM image of the RT-$MAPbI_3$ film deposited on glass substrate for PL measurements. The image employs a 1 µm scale bar.

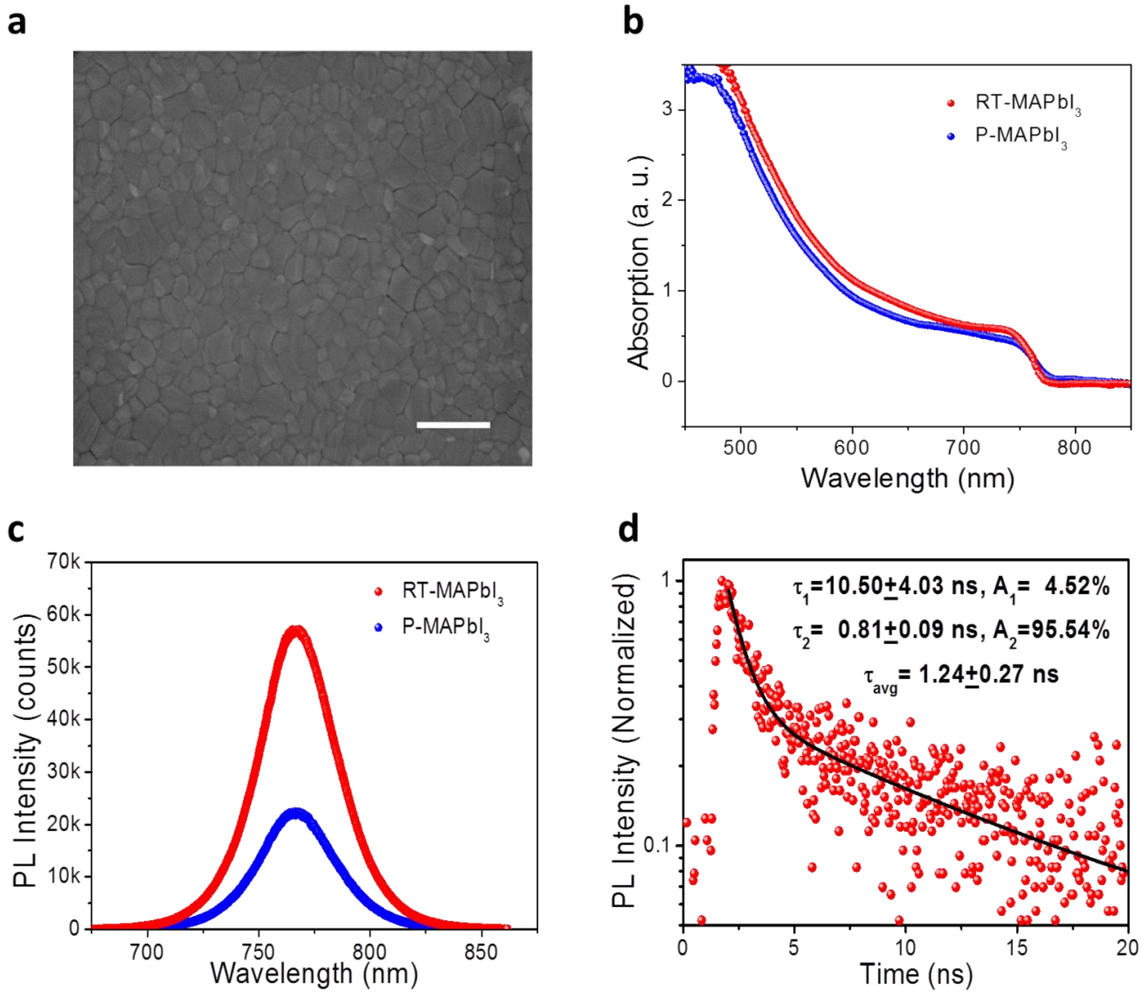

Fig. S5. a, Top-view SEM image of the P-MAPbI$_3$ film deposited on a glass substrate for PL/TRPL measurements. The image employs a 1 µm scale bar; **b-c**, UV-Vis (**b**) and PL (**c**) spectra of the RT-MAPbI$_3$ and P-MAPbI$_3$ films; **d**, TRPL spectra of the P-MAPbI$_3$ film. The excitation wavelength for the PL spectrum is 442 nm and the excitation for TRPL is 405 nm. The charge carrier lifetimes (τ_1 and τ_2) and their corresponding contributions (A_1 and A_2) are extracted by fitting the PL decay curves with a biexponential equation.

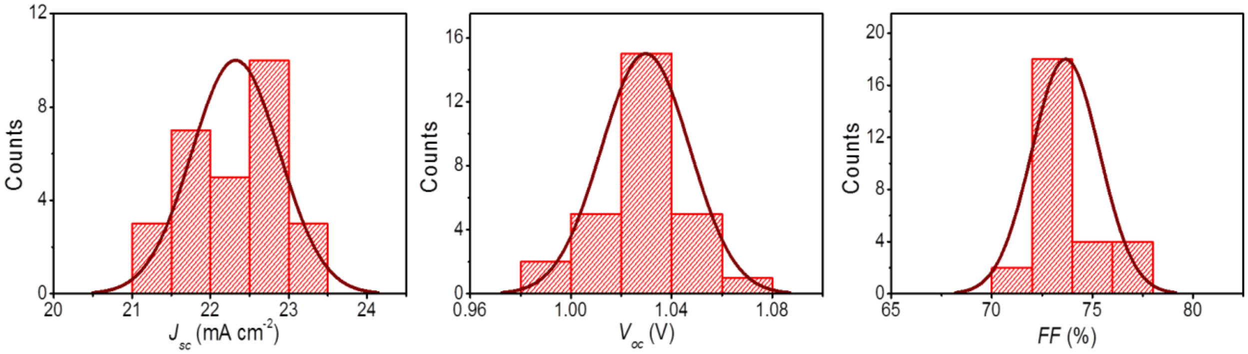

Fig. S6. Statistical J_{sc}, V_{oc} and *FF* of devices prepared using RT-MAPbI$_3$ films. The *J*-*V* measurement was conducted in air (relative humidity of 35~55%), with 0.1 V s^{-1} voltage scanning rate and forward scanning direction.

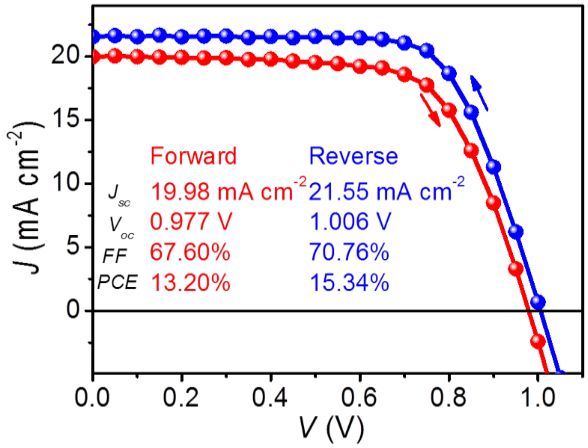

Fig. S7. *J*-*V* characteristics of the best-performing device achieved with a P-MAPbI$_3$ film. The *J*-*V* characteristics were obtained by both forward and reverse scanning direction with 0.1 V s^{-1} scanning rate.

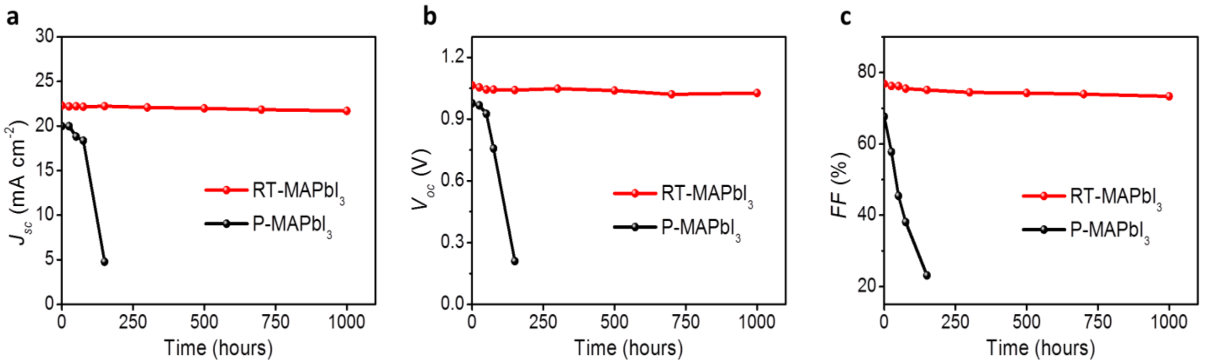

Fig. S8. J_{sc}, V_{oc} and FF of best-performing devices prepared using RT-MAPbI$_3$ and P-MAPbI$_3$ films, as a function of time. The devices were stored without encapsulation under relative humidity of 20~25%. The *J-V* measurement was conducted with 0.1 V s^{-1} voltage scanning rate and forward scanning direction.

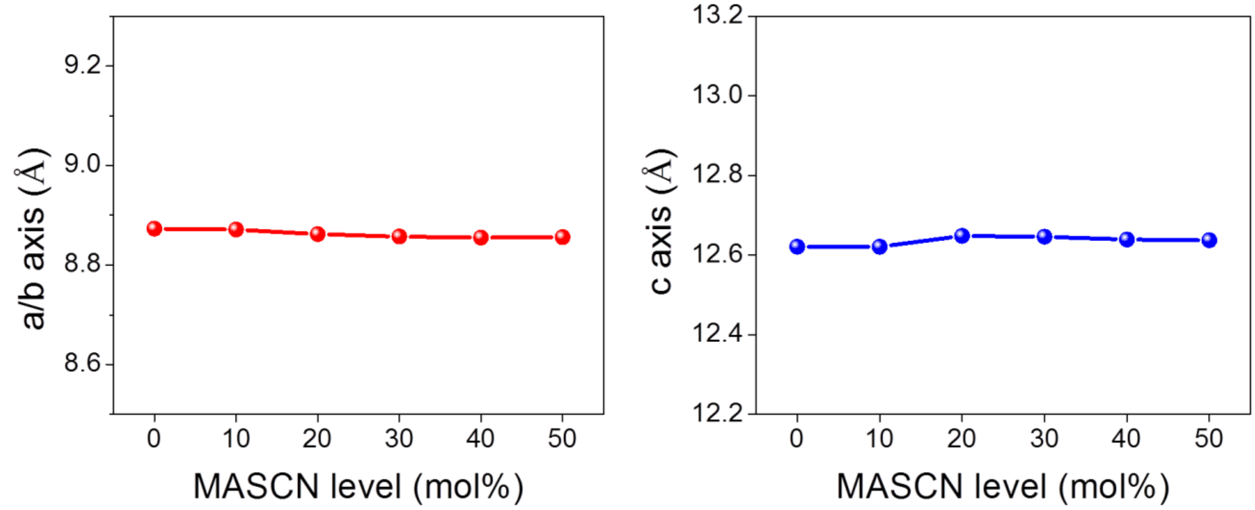

Fig. S9. The unit cell parameters (determined from full-profile Pawley fitting) as a function of MASCN additive level to the RT-MAPbI$_3$ film precursor solution.

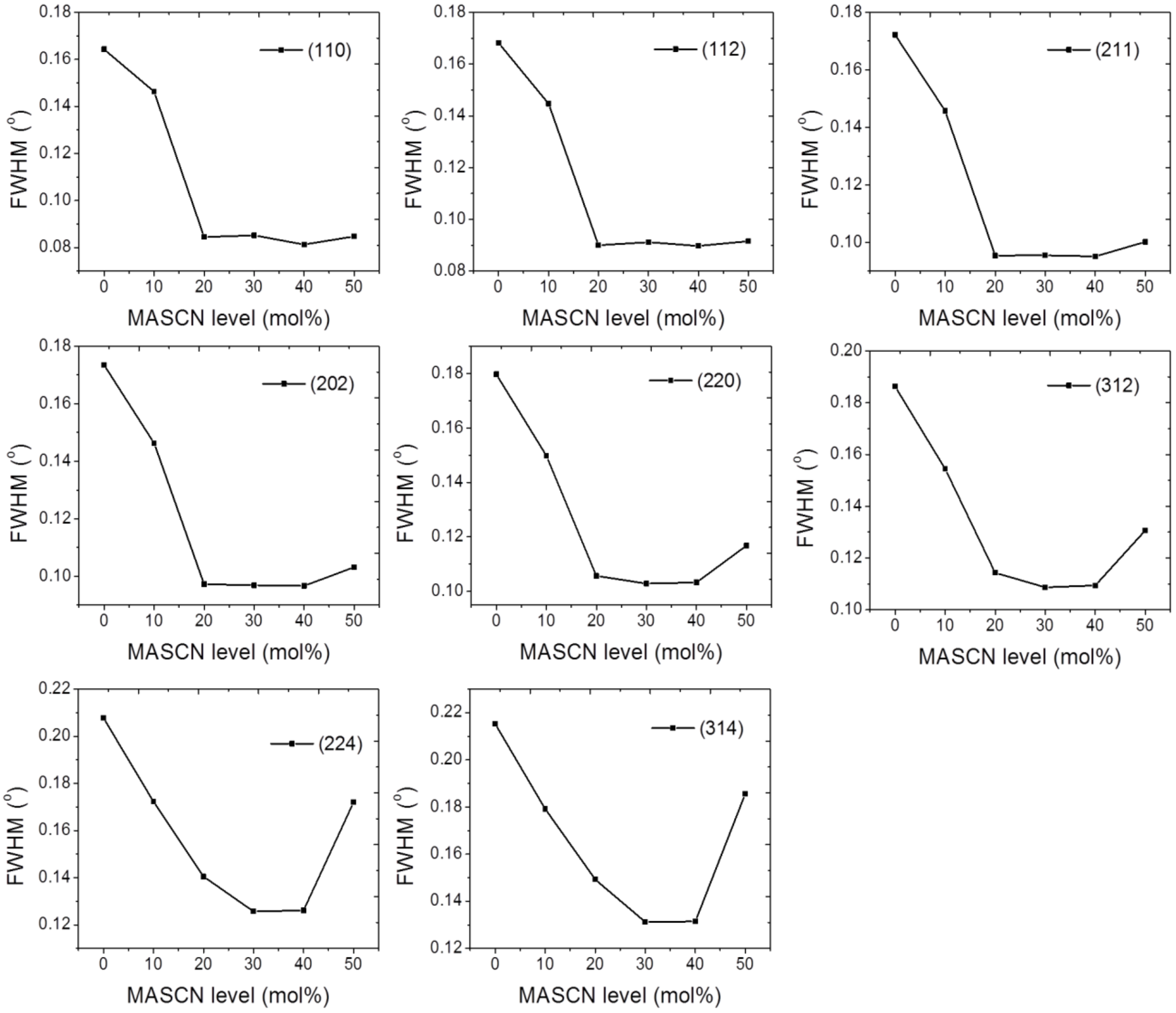

Fig. S10. FWHMs of specified XRD peaks for RT-MAPbI$_3$ films as a function of MASCN additive level.

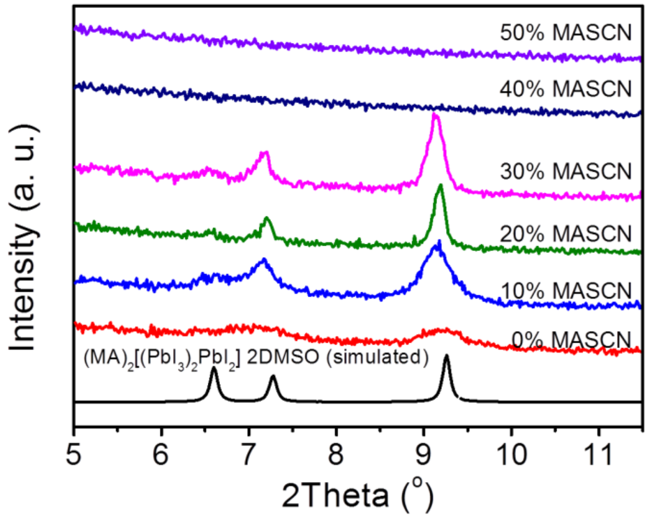

Fig. S11. Zoomed-in XRD pattern, focusing on the 5-12° 2θ range, for RT-MAPbI$_3$ films with 5% extra PbI$_2$ and 0~50% MASCN addition in the precursor solutions. The simulated XRD pattern for (MA)$_2$[(PbI$_3$)$_2$PbI$_2$]•2DMSO is also included for comparison. The structure of (MA)$_2$[(PbI$_3$)$_2$PbI$_2$]•2DMSO is shown in Fig. S10 (ESI†).

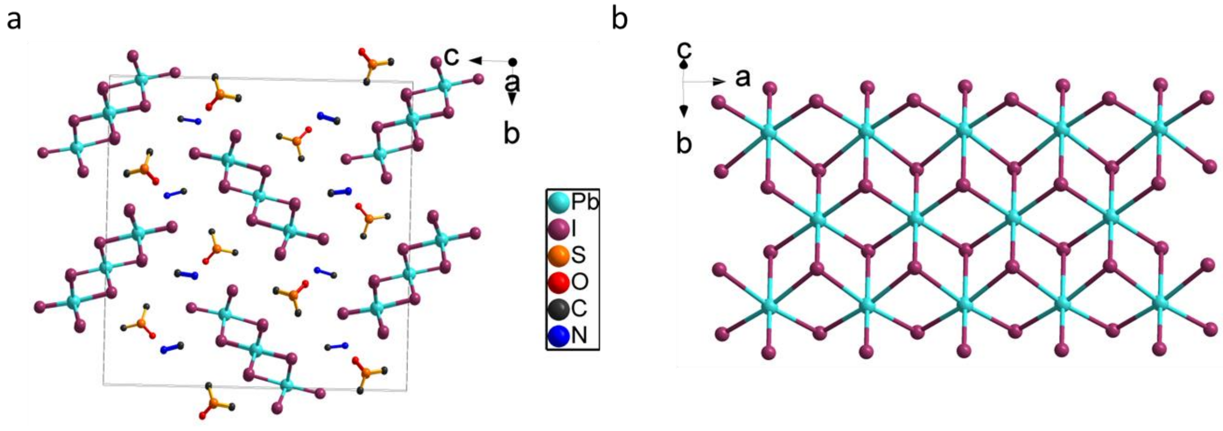

Fig. S12. Schematics of (**a**) the packing structure of (MA)$_2$[(PbI$_3$)$_2$PbI$_2$]•2DMSO and (**b**) the 1D structure of [(PbI$_3$)$_2$PbI$_2$]$^{2-}$ along different crystallographic directions. The corresponding simulated XRD pattern for (MA)$_2$[(PbI$_3$)$_2$PbI$_2$]•2DMSO is shown in Fig. S9.

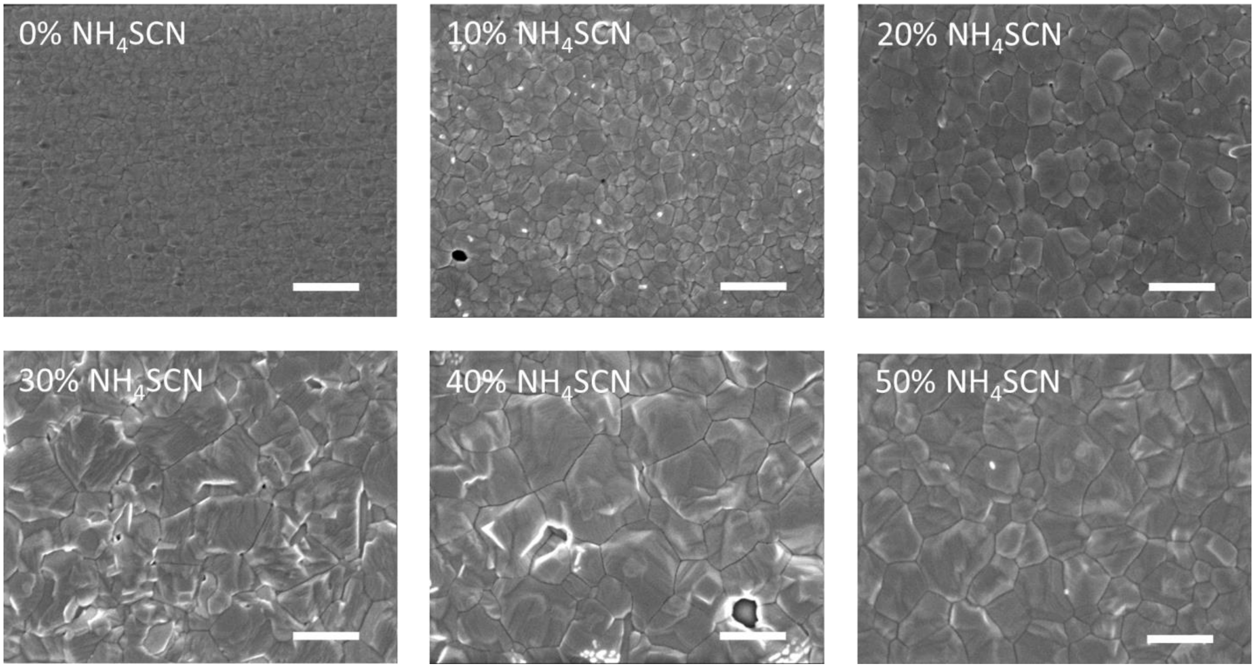

Fig. S13. Top-view SEM images of the room-temperature $MAPbI_3$ films with 5% extra PbI_2 and 0~50% NH_4SCN addition to the $MAPbI_3$ precursor solutions. All films were deposited on glass/FTO/TiO_2 substrates and all images employ a scale bar of 1 µm.

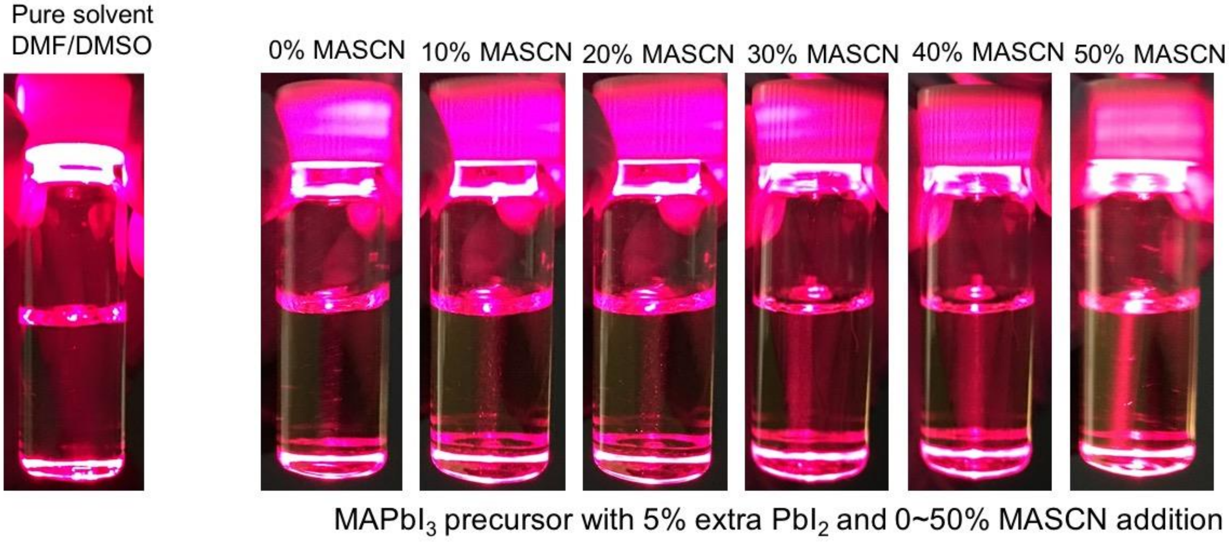

Fig. S14. Tindall test of DMF/DMSO solvent and $MAPbI_3$ precursor solutions with 5% extra PbI_2 and 0~50% MASCN addition. The DMF/DMSO solvent does not show the Tindall effect, but all the $MAPbI_3$ precursor solutions do show the Tindall effect. The red laser illuminates from the bottom of the vials.

Supplementary Tables

MASCN addition level (%)	**a/b axis (Å)**	**c axis (Å)**
0	8.873(2)	12.621(4)
10	8.871(1)	12.621(2)
20	8.862(1)	12.648(1)
30	8.857(1)	12.646(1)
40	8.855(1)	12.639(1)
50	8.856(1)	12.637(1)

Table S1. The unit cell parameters list (determined from full-profile Pawley fitting) as a function of MASCN additive level to the $MAPbI_3$ film precursor solution.

MASCN addition level (%)	V_{oc} (V)	J_{sc} (mA cm^{-2})	*FF* (%)	*PCE* (%)
0	0.638	8.78	36.48	2.04
10	0.893	17.61	52.16	8.20
20	0.986	19.97	54.52	10.74
30	0.997	19.86	70.76	14.02
20	0.986	19.97	54.52	10.74
40	1.064	22.29	76.83	18.22
50	1.000	22.54	76.64	17.27

Table S2. The photovoltaic parameters of the best-performing solar cells prepared using RT-$MAPbI_3$ films with 5% extra PbI_2 and 0~50% MASCN addition to the $MAPbI_3$ precursor solution. All *J-V* measurements were conducted with 0.1 V s^{-1} voltage scanning rate and forward scanning direction.

References

1. W. Ke, C. Xiao, C. Wang, B. Saparov, H. S. Duan, D. Zhao, Z. Xiao, P. Schulz, S. P. Harvey and W. Liao, Adv. Mater., 2016, 28, 5214-5221.
2. N. J. Jeon, J. H. Noh, Y. C. Kim, W. S. Yang, S. Ryu and S. I. Seok, Nat. Mater., 2014, 13, 897-903.